Electron-impact single ionization of W^{19+} ions

Alexander Borovik, Jr.,[1,2,*] Benjamin Ebinger,[1,2] Daniel Schury,[1,3] Stefan Schippers,[1,2] and Alfred Müller[1]

[1]*Institut für Atom- und Molekülphysik, Justus-Liebig Universität Giessen, Giessen, Germany*

[2]*I. Physikalisches Institut, Justus-Liebig Universität Giessen, Giessen, Germany*

[3]*GSI Helmholtzzentrum für Schwerionenforschung GmbH, Darmstadt, Germany*

(Received 2 December 2015; published 19 January 2016)

Electron-impact single ionization of W^{19+} ions has been studied both experimentally and theoretically. By employing the crossed-beams method, absolute cross sections have been measured in the energy range from the ionization onset up to 1000 eV. Theoretical calculations of the ionization-cross-section function were performed using the configuration-averaged distorted-wave method for electron-ion collision energies up to 150 keV. Contributions of excited long-lived primary-ion-beam admixtures were taken into account. The role of different competing ionization mechanisms contributing to the studied cross section is discussed. Plasma rate coefficients have been inferred and are presented in parametrized form.

DOI: 10.1103/PhysRevA.93.012708

I. INTRODUCTION

Tungsten, due to its robustness and stability, has been chosen as the material for plasma-facing surfaces in tokamaks. However, as a result of the high particle flux to surfaces, sputtering of tungsten atoms and ions and their entry into the tokamak plasma is unavoidable. Tungsten atoms and ions with their high collisional cross sections and wide ranges of charge states and excitations are very effective energy absorbers and may lead to strong radiation losses eventually preventing the thermonuclear reaction from ignition [1]. Highly sophisticated modeling is being performed to predict the behavior of tungsten impurities and their influence on the tokamak plasma [2]. The model calculations require a huge amount of high-precision input data including, among others, information on elementary processes for tungsten ions in all ionization stages. The present study addresses the process of single ionization of W^{19+} ions by electron impact and is a part of a project [3] which combines investigations of electron-impact ionization [4], dielectronic recombination [5,6], and photoionization [7] of low and intermediately charged tungsten ions.

Electron-impact ionization of atoms and ions of the tungsten isonuclear sequence has been and remains to be a subject of intensive research using both experimental and theoretical approaches. To our knowledge, no experimental study on the electron-impact ionization of neutral tungsten atoms has been reported in the literature. A theoretically calculated ionization cross section for neutral tungsten has been reported by Pindzola and Griffin [8]. Montague and Harrison presented an experimental study of single ionization of W^+ ions [9]. More than 10 years later Stenke *et al.* measured cross sections for single ionization of W^+ through W^{10+} [10] and for double ionization of W^+ through W^{6+} together with triple ionization of W^+ through W^{4+} [11]. Kwon *et al.* have calculated ionization cross sections of W^+ as well as of neutral tungsten atoms [12]. Ballance *et al.* have calculated ionization cross sections of W^{3+} using both level-to-level R-matrix and configuration-averaged distorted wave (CADW) methods [13]. Calculations of single-ionization cross sections of W^{4+}, W^{5+}, and W^{6+} ions were performed by Pindzola and Griffin [14]. Single- and double-ionization cross sections of W^{17+} have been measured by Rausch *et al.* [4]. A theoretical study on single ionization of W^{17+} has been presented by Zhang and Kwon [15]. Contributions of high-nl subshells to the single ionization of W^{27+} were theoretically investigated by Jonauskas *et al.* [16]. A systematic theoretical study of single-ionization cross sections for all tungsten ionization stages has been performed by Loch *et al.* [17]. Another systematic theoretical work on single ionization of W^+ through W^{63+} has been recently reported by Demura *et al.* [18]. Double ionization of tungsten atoms as well as of ionization stages 2, 4, and 6 has been calculated by Jonauskas *et al.* [19]. Detailed information on energy levels of tungsten in various charge states together with the recommended values of potentials for ionization from the ground states were compiled by Kramida and Shirai [20–22] and are made available in the NIST Atomic Spectra Database (NIST ASD) [23].

In the present paper we report on both experimental and theoretical single-ionization cross sections of W^{19+}. The remainder of the paper is organized as follows: the following section describes the employed apparatus and the experimental conditions. Section III gives a short overview of the theoretical approach. The results obtained for cross sections and plasma rate coefficients are presented and discussed in Sec. IV. Conclusions are provided in Sec. V.

II. EXPERIMENTAL SETUP

The single-ionization cross section of W^{19+} has been measured using the Giessen crossed-beams setup [24,25]. Details of the experimental procedures [4,26] have been given previously. Therefore, only a brief overview will be provided here. Absolute cross sections were measured using the well-established animated-beam technique [27–29]. In addition, a fine-step energy-scan technique was employed to uncover details in the energy dependence of the measured cross section [30–32]. The present setup has been successfully used for studies of ionization cross sections of a wide range of ions ([33] and references therein) and the recent measurements on N^{5+} ions [34] illustrate the level of the obtainable data quality.

*Alexander.Borovik@iamp.physik.uni-giessen.de

W^{19+} ions were produced by introducing tungsten-hexacarbonyl, $W(CO)_6$, vapor into the plasma chamber of a 10-GHz ECR ion source through a fine-regulation gas valve. Because of tungsten film depositions onto the inner surfaces of the ion source, including the vacuum gauge, the measurement of the pressure inside the ion source was distorted and, consequently, no exact value can be provided. Such depositions were also the reason for frequent discharges and resulting ion-beam instabilities, which made the ion-beam production difficult. The total ion composition was extracted from the ion source with a voltage of 12 kV and was mass-over-charge analyzed in the field of the first dipole magnet, The desired isotope-resolved $^{186}W^{19+}$ ions were isolated. Before entering the interaction region, the primary ion beam was collimated by two pairs of four-jaw slits separated from one another by 195 mm. The resulting ion current in the interaction region varied between 1.2 and 1.7 nA, at a beam size of 1×1 mm^2. Such tight beam collimation ensured the complete collection of the product ion beam in the single-particle detector and of the primary ion beam in the Faraday cup. For fine-step energy scans this condition could be relaxed: the slit size was increased to 1.5×1.5 mm^2, which resulted in a primary ion current of 3.1 nA available for the measurement. In the interaction region, the ion beam was crossed by a ribbon-shaped electron beam produced by a high-power electron gun [35]. The resulting product-ion count rate did not exceed 300 W^{20+} ions per second. The signal-to-background ratio varied from 1.6 at 500 eV to 8 at 950 eV.

The systematic uncertainty of the absolute cross-section measurement has been calculated as the quadrature sum of uncertainties of the parameters included in the cross-section evaluation. In the present measurement, this was determined to be 6.6%. Statistical uncertainties were better than 2% for measurements well above the ionization onset. The square root of the sum of squares of all uncertainties, i.e., the total uncertainty of the measurement, equals to about 7% beyond 650 eV. Details considering the error budget, as well as details on the cross-section determination procedure have been provided previously [4]. Statistical uncertainties of the energy-scan measurement at energies well above the ionization onset are 1.5% or less.

III. THEORETICAL METHOD

The approach employed to calculate cross sections for single ionization of W^{19+} ions is identical to the one successfully used in analogous studies of ions belonging to the $4d$-open-shell xenon and tin isonuclear sequences [33,36] and similar to the one employed by Loch *et al.* [17]. The total electron-impact single-ionization cross section has been treated as a sum of contributions of *direct ionization* (DI) and indirect *excitation-autoionization* (EA) processes,

$$\sigma_{\rm ion}^{i} = \sigma_{\rm dir}^{i} + \sum_{j} \sigma_{\rm exc}^{i\to j} B_j^a, \tag{1}$$

where $\sigma_{\rm dir}^{i}$ is the cross section for direct removal of an electron from the initial configuration i by the incident electron. The second term in the expression, representing the excitation-autoionization contribution, is the sum of cross sections for promotions from the initial configuration i to a higher configuration j multiplied by the branching ratio for autoionization B_j^a, which is the probability for the configuration j to decay via Auger processes and, hence, for being able to contribute to net single ionization. Supported by the suggestion of Loch *et al.* [17] and aiming at keeping the calculational efforts within a reasonable frame, we chose B_j^a to be unity for all j with excitation energies above the ionization potential.

For the case when an excited long-lived ion component is present in the parent ion beam used in the experiment, the total cross section compared with the experimental data is calculated as

$$\sigma_{\rm ion} = \left(1 - \sum_{E} k^E\right)\left(\sigma_{\rm dir}^{G} + \sum_{j} \sigma_{\rm exc}^{G\to j}\right) + \sum_{E} k^E \left(\sigma_{\rm dir}^{E} + \sum_{j} \sigma_{\rm exc}^{E\to j}\right), \tag{2}$$

where $\sigma_{\rm dir}^{G}$ and $\sigma_{\rm exc}^{G\to j}$ are the cross sections for DI and EA of ground-state ions, while $\sigma_{\rm dir}^{E}$ and $\sigma_{\rm exc}^{E\to j}$ are the cross sections of DI and EA for long-lived excited ions, respectively. k^E represents the relative amount of an excited-ion component in the primary ion beam of the measurement. The present experimental data do show evidence of such ion-beam components.

Cross sections $\sigma_{\rm dir}$ and $\sigma_{\rm exc}$ have been calculated using the configuration-averaged distorted wave (CADW) approach implemented in the Los Alamos National Laboratory Atomic Physics Code Package (see Sec. 2.1 in [37]), which is available online [38]. For the $4d^{10}4f^9$ ground-state configuration of W^{19+}, we have included all EA processes involving excitations $4d, 4p, 4s \to nl$, with $5 \leqslant n \leqslant 13$. For the excited $4d^{10}4f^8 5s$ configuration of W^{19+}, excitations $4f \to nl$ with $12 \leqslant n \leqslant 23$ have been taken into account in addition to the excitations $4d$, $4p$, and $4s \to nl$ ($5 \leqslant n \leqslant 13$). In all cases, all orbital quantum numbers $l \leqslant 6$ were included. The highest principal quantum number $n_{\rm max} = 13$ and $n_{\rm max} = 23$ for the ground and excited configurations, respectively, in the present work, are still lower than those in the studies of Zhang and Kwon on W^{17+} [15] and of Jonauskas *et al.* on W^{27+} [16] but are assumed to provide almost converged results.

Higher-order processes such as *resonant-excitation double autoionization* (REDA [39]) are negligibly small for W^{17+} according to Zhang and Kwon [15]. The experimental cross-section energy scan for W^{17+} by Rausch *et al.* [4] did not show any evidence of resonance structures. In the present energy scan for W^{19+}, no resonance structures can be observed either. Therefore, we do not expect REDA processes to contribute significantly to the studied cross-section function. Consequently, REDA has not been considered in the present calculations.

IV. RESULTS

A. Cross section

In the frame of the present study, the cross section for electron-impact single ionization of W^{19+} has been measured in the energy range from the observed onset up to 1000 eV and

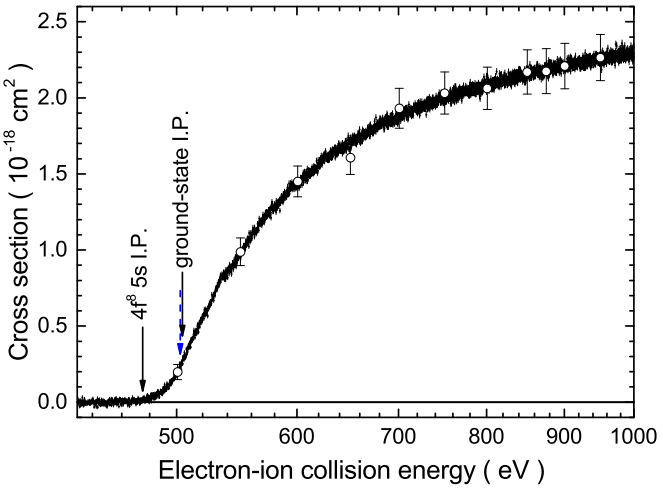

FIG. 1. The experimentally measured electron-impact single-ionization cross section of W^{19+}: open circles are absolute cross-section data with total experimental error bars, the thin solid line represents the result of the energy scan. Solid vertical arrows show threshold energies for ionization from the ground level of W^{19+} and from the lowest level in the $4d^{10}4f^{8}5s$ excited configuration of W^{19+} calculated using the Cowan code [41]. The dashed (blue) vertical arrow represents the value of the ground-state ionization potential from the NIST Atomic Spectra Database [23].

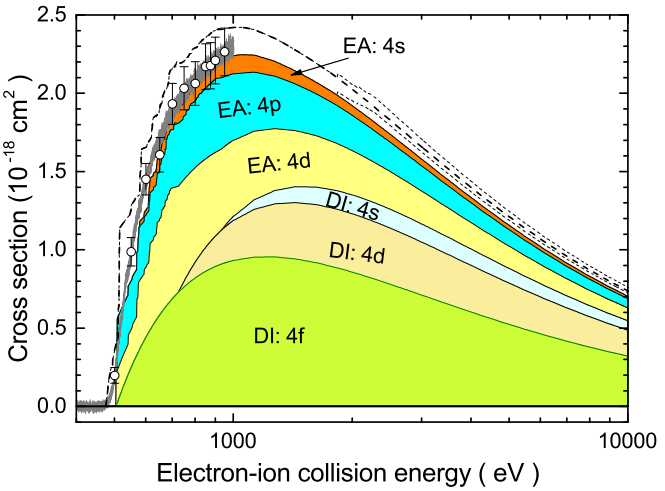

FIG. 2. Comparison of the present experimental and theoretical (CADW) electron-impact single-ionization cross sections of W^{19+}. Open circles are absolute cross-section data; the grey thin solid line represents the energy scan. Calculated contributions of DI and EA processes for ground-configuration $4d^{10}4f^{9}$ W^{19+} ions are represented by the differently shaded (colored) areas. The calculated total cross section of W^{19+} in the excited $4d^{10}4f^{8}5s$ electron configuration is represented by the thick dashed curve. Thin dashed curves on top of the two total cross sections, in addition, include excitations from the $3d$ subshell (at energies beyond approximately 1800 eV) which most likely contribute only to net multiple ionization.

is shown in Fig. 1. The cross-section function has a mostly smooth shape over the whole experimentally investigated energy range with small step features at energies from the onset up to 700 eV. The highest measured cross section is approximately 2.3×10^{-18} cm^2 at 1000 eV. This value, however, does not correspond to the maximum of the cross-section function, which we expect to appear beyond the experimentally available energy range. The ionization cross section has been calculated by Loch *et al.* [17] and Demura *et al.* [18], but no data in the form of a cross section versus electron energy have been made available. Loch *et al.* provided Maxwellian-averaged plasma rate coefficients (PRCs) [40], which will be compared with the presently inferred PRCs in Sec. IV B.

The ionization onset of the present experimental cross section is observed at around 470 eV, which is lower than both the ground-state ionization threshold calculated using the atomic structure code of Cowan [41] (504.39 eV) and the ionization-potential value in the NIST Atomic Spectra Database [23] (502.6 eV), meaning that excited long-lived ion species with excitation energies of up to 32–34 eV were present in the experiment. The observed ionization onset agrees with the ionization potential of W^{19+} in the lowest excited configuration $4d^{10}4f^{8}5s$ (474.91 eV according to a configuration-averaged calculation with the Cowan code). Excited levels of the next higher excited configuration $4d^{10}4f^{8}5p$ are in the range around 64–134 eV. Their presence in the primary ion beam should have caused ionization to start at around 440 eV, which was not observed in the experiment. The $4d^{10}4f^{9}$ ground configuration of W^{19+}, however, contains 198 levels spread over the range of almost 37 eV all of which must be assumed to be long-lived since no electric dipole transitions between them are allowed. In this situation, we assume that W^{19+} ions in long-lived excited levels of the ground configuration have been admixed to the ground-level primary ion beam. At the same time we cannot exclude that W^{19+} ions in the $4d^{10}4f^{8}5s$ electron configuration were present in the experiment as well and also contributed to the measured cross section.

In many-electron systems, such as W^{19+}, electron-impact ionization results from a variety of competing ionization mechanisms involving electrons of outer and inner subshells [39]. In order to shed light on the contributions from different subshells in the single ionization of W^{19+}, we have calculated the cross section employing the CADW method as described in Sec. III considering both the $4d^{10}4f^{9}$ ground and $4d^{10}4f^{8}5s$ excited configuration. Figure 2 shows the calculated cross sections in comparison with the present experimental results. The differently shaded areas represent contributions of competing ionization mechanisms involving the indicated electron subshells of the ground-configuration $4d^{10}4f^{9}$ W^{19+} ion. The cross section for W^{19+} in the $4d^{10}4f^{8}5s$ excited configuration is represented by the thick dashed curve. The calculated cross section for the ground configuration is in very good agreement with the experimental data at energies from approximately 650 to 1000 eV. At lower energies, small discrepancies are found, which most probably originate from the discrete-step behavior of the calculated cross section due to the employed configuration-average approach instead of a gradual increase associated with the many individual excited levels. The calculated cross section for the $4d^{10}4f^{8}5s$ excited configuration is slightly above the experimental data, but the difference between them, at higher energies, is approximately equal to the experimental error bars.

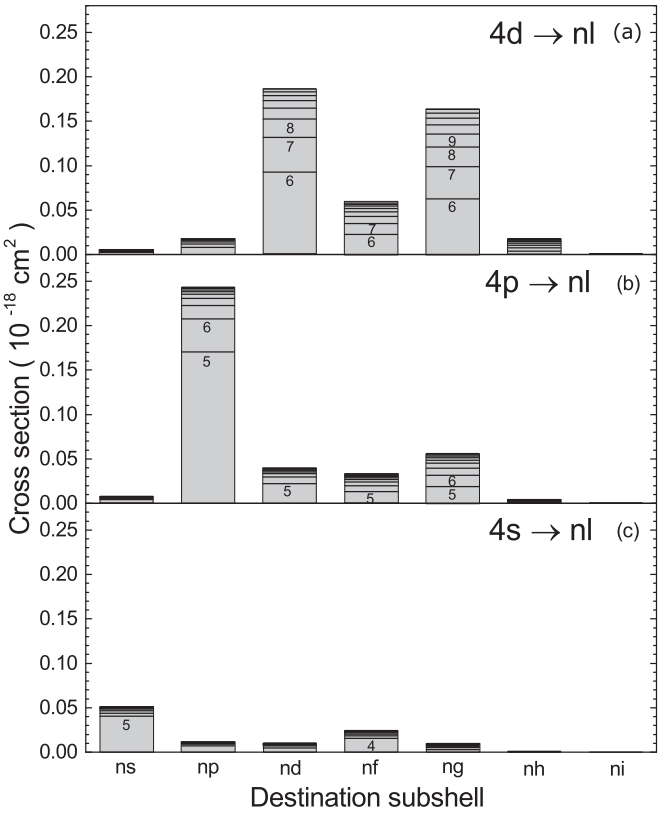

FIG. 3. Contributions of EA processes from excitation of the $4d$ (a), $4p$ (b), and $4s$ (c) subshells to the cross section of ground-configuration W^{19+} at its calculated maximum (1100 eV). For each angular momentum l considered, the contributions by excitations to the various principal quantum numbers n are labeled accordingly.

For W^{19+} in the ground configuration, DI clearly dominates the total cross section at higher energies. The largest contribution is produced by the process of direct removal of an electron from the $4f$ subshell. DI contributions of other subshells are significantly weaker. At lower energies down to the ionization onset, contributions of EA are of the same importance as those of DI. EA is mainly associated with excitations of the $4d$ and $4p$ subshells, whose contributions are almost equal in magnitude. Contributions of the EA processes involving excitations of the $4s$ subshell are smaller. In excited $4d^{10}4f^{8}5s$ W^{19+} ions, relative contributions to the total cross section are similar with only few differences: excitations of the $4f$ subshell to high nl lead to the formation of autoionizing states and, thus, constitute an additional EA channel. This results in the overall EA contribution dominating the total ionization cross section of $4d^{10}4f^{8}5s$ W^{19+} at energies up to 900 eV. Above this energy, EA contributions decrease and DI becomes dominant.

Figure 3 shows histograms illustrating the contributions of single excitations from the $4d$, $4p$, and $4s$ to various nl subshells to the calculated cross section of ground-configuration W^{19+} at its maximum, which is found at 1100 eV. Excitations from the $4d$ subshell to nd, nf, and ng provide the strongest contributions. The promotion $4p \rightarrow 5p$ yields about half of the total contribution arising from all $4p \rightarrow nl$ EA processes. Excitations $4p \rightarrow nd$, $4p \rightarrow nf$, and $4p \rightarrow ng$ also invoke

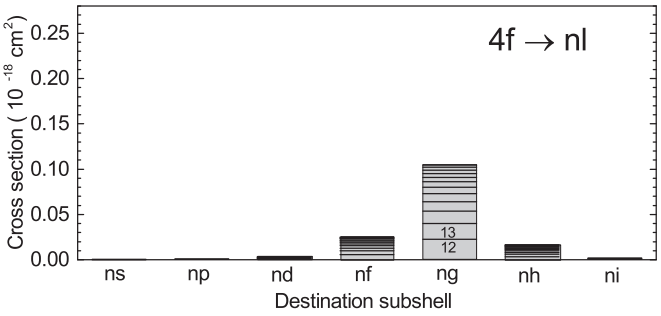

FIG. 4. Contributions of EA processes from excitation of the $4f$ subshell to the cross section of $4d^{10}4f^{8}5s$ excited-configuration W^{19+} ions at its calculated maximum (1100 eV). For each angular momentum l considered, the contributions by excitations to the various principal quantum numbers n are labeled accordingly.

considerable contributions to net single ionization. Among the $4s$ excitations, only promotions to the $5s$ and $4f$ subshells produce visible contributions. For W^{19+} in the $4d^{10}4f^{8}5s$ excited configuration, relative contributions of excitations to different nl forming vacancies in the $4d$, $4p$, and $4s$ subshells are very similar to those in Fig. 3 and, therefore, are not shown separately. Figure 4 shows contributions of the EA processes, which involve excitations of the $4f$ subshell of excited-configuration W^{19+} ions. Here, contributions due to promotions to ng subshells clearly dominate.

Finally, we have also estimated cross sections for excitation of the $3d$ subshell (shown in Fig. 2 by the thin dashed lines for both ground- and excited-configuration ions). These processes occur at energies far beyond the threshold for the ionization of the next following charge state W^{20+} (1046 eV [23]) and, therefore, should mostly contribute to the double-ionization cross section of W^{19+}. The electron energies at which these processes occur were beyond the energy range available in the present experiment. Hence, no search for the corresponding structure in the cross section by a fine-step energy scan could be provided. However, since the calculated $3d$ excitation cross sections are relatively very small, considering what has been discussed above, their contribution to net single ionization can only be overestimated. Therefore, all processes involving excitation of the $3d$ subshell were left out of further considerations.

B. Plasma rate coefficients

Aiming at an easy implementation of the present results in plasma modeling, plasma rate coefficients (PRCs) from the presently studied single-ionization cross section of W^{19+} have been derived. The employed procedure is identical to the one previously used for xenon and tin ions [33,36]. The ionization cross section σ is multiplied by the electron-ion relative velocity v and the product $v\sigma$ is integrated over a Maxwellian velocity distribution [42].

Figure 2 suggests that the ground configuration of W^{19+} predominantly contributes to the measured single-ionization cross section. Contributions of the $4d^{10}4f^{8}5s$ excited configuration of W^{19+} are considered to be of minor significance. Therefore, we treated the experimental cross section as that of

the ground configuration of W^{19+} and used it to infer the PRC for single ionization.

We have checked which energy range of the electron-impact ionization cross section has to be included in the integration of $v\sigma$ over electron temperature in order to obtain converging plasma rate coefficients. In agreement with Fogle *et al.* [43], we find that for a given electron temperature T_e the cross section must be known in the energy range from the ionization threshold up to approximately $6k_BT_e + I_{eV}$, where I_{eV} is the ionization potential and k_B Boltzmann's constant. In the present experiment, electron energies up to 1000 eV have been available, which enabled us to derive plasma rate coefficients for the electron temperature range up to about 9.63×10^5 K (83 eV). In a tokamak, like ITER, the expected electron temperatures in the region of the divertor electrodes are 0.1–100 eV [44], however, in the regions towards the core plasma, electron temperatures should reach 20–25 keV [2]. Therefore, in order to provide PRCs in an extended electron-temperature range, the present experimental data had to be extrapolated. This was done by merging the experimental data with the CADW calculations performed for collision energies up to 150 000 eV. The latter was normalized to the experiment by multiplying it with the factor of 1.02. We have also derived the PRC for the excited $4d^{10}4f^85s$ W^{19+} using the calculated CADW data directly. The uncertainty for the PRC of the ground-configuration W^{19+} corresponds to that of the experimental cross sections and equals to approximately 7%. The uncertainty of the PRC for the excited $4d^{10}4f^85s$ W^{19+} depends on the accuracy of the theoretical description of the cross section by the employed CADW approach. However, taking into account the good agreement observed in Fig. 2, we do not expect it to exceed 10%.

Figure 5 shows the present PRCs for W^{19+} in the ground electron configuration as well as for W^{19+} in the $4d^{10}4f^85s$ first excited configuration together with the previous data of

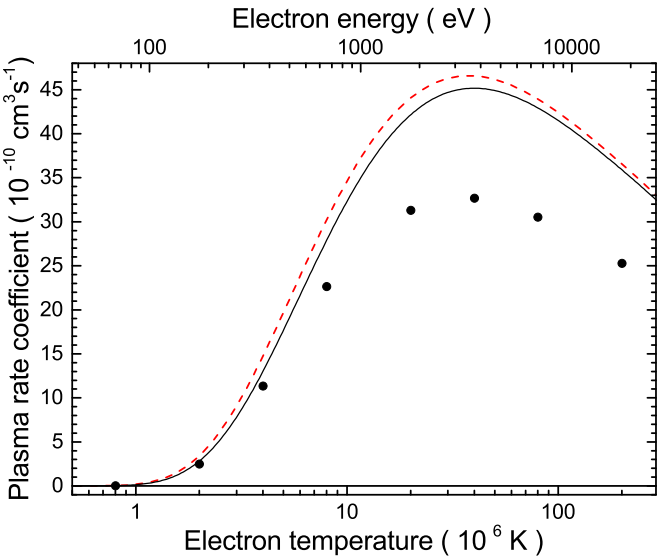

FIG. 5. Present plasma rate coefficients for electron-impact single ionization of W^{19+} ions in the ground configuration (black solid curve) and in the $4d^{10}4f^85s$ excited configuration (red dashed curve). The black dots represent the data of Loch *et al.* [17] taken from [40].

TABLE I. Fitting parameters a_i of the fifth-order polynomial $\alpha(T_e) = \sum_{i=0}^{5} a_i T_e^i$ and scaling parameters E_0 to reproduce the scaled plasma rate coefficients for single ionization of W^{19+} ions in ground and in the $4d^{10}4f^85s$ excited configuration. The numbers in square brackets are powers of 10 to be multiplied with the preceding numbers, respectively.

W^{19+}	$4d^{10}4f^9$	$4d^{10}4f^85s$
E_0	468.80	474.40
a_0	1.70703[-5]	1.58871[-4]
a_1	1.11227[-3]	3.02933[-4]
a_2	6.63615[-3]	7.08722[-4]
a_3	1.90504[-2]	1.13211[-3]
a_4	2.64960[-2]	1.04854[-3]
a_5	1.42295[-2]	4.40051[-4]

Loch *et al.* [17] taken from the CFADC database [40]. The presently derived PRC data show relatively little difference from one another, approximately 3% near their maximum at around 4×10^7 K. Considering the estimated uncertainties, they may be treated as indistinguishable. The data of Loch *et al.* [17] are lower than both of the present PRC data sets at temperatures beyond 5×10^6 K. The probable reason for the observed discrepancy is the fact that in their calculations Loch *et al.* have considered a relatively low number of inner-shell excitations contributing to EA ($n \leqslant 8$ and $l \leqslant 3$). Thus, their calculated ionization cross section is too small and results in too low PRCs. A similar suggestion has been made by Zhang and Kwon [15] considering the case of the W^{17+} ion. Only in the electron-temperature range $(1–3) \times 10^6$ K, where the highest abundance of W^{19+} in a tokamak plasma has been predicted [45], are the present data and the data of Loch *et al.* in good agreement with one another.

We have scaled the present PRCs using the Burgess-Tully model reported by Dere [46]. The electron temperature has been scaled as

$$x = 1 - \frac{\ln 2}{\ln(t+2)} \tag{3}$$

with $t = k_BT_e/E_0$. The PRCs have been scaled as

$$\rho = t^{1/2}E_0^{3/2}\alpha(T_e)/E_1(1/t), \tag{4}$$

where $E_1(1/t)$ is the first exponential integral. Here, the quantity E_0 is considered as a scaling parameter and slightly differs from the experimentally measured ionization threshold. The scaled plasma rate coefficients have been fitted by a fifth-order polynomial $\alpha(T_e) = \sum_{i=0}^{5} a_i T_e^i$ with fitting parameters a_i $(i = 0, \ldots, 5)$. In the temperature range shown in Fig. 5, the fits reproduce the derived plasma rate coefficients with an accuracy of 2% or better. The sets of resulting parameters a_i are listed in Table I.

V. CONCLUSIONS

Single ionization of W^{19+} ions has been investigated employing both experimental and theoretical approaches. A systematic analysis of the roles of competing ionization

mechanisms has been carried out showing the high importance of indirect ionization processes. Admixtures to the parent ion beam in the experiment of excited ions have been considered. Plasma rate coefficients for W^{19+} ions in the ground- and in the first excited electron configuration have been inferred. These are up to 40% larger than the results of previous calculations. The reason for this discrepancy is most likely in the neglect of excitation-autoionization contributions involving intermediate configurations with high principal and orbital angular momentum quantum numbers n and l, respectively, in the older calculations. These findings suggest that previously recommended PRCs for ionization of W^{19+} ions should be replaced by our data. Therefore, the present PRC values have been parametrized for easy implementation in plasma modeling codes and the parameters are provided in tabular form.

ACKNOWLEDGMENT

The present study was performed with support by the Deutsche Forschungsgemeinschaft under Project No. Mu1068/20.

[1] A. Kallenbach, R. Neu, R. Dux, H.-U. Fahrbach, J. C. Fuchs, L. Giannone, O. Gruber, A. Herrmann, P. T. Lang, B. Lipschultz, C. F. Maggi, J. Neuhauser, V. Philipps, T. Püterich, V. Rohde, J. Roth, G. Sergienko, A. Sips, and ASDEX Upgrade Team, Plasma Phys. Controlled Fusion **47**, B207 (2005).

[2] G. Hogeweij, V. Leonov, J. Schweinzer, A. Sips, C. Angioni, G. Calabrò, R. Dux, A. Kallenbach, E. Lerche, C. Maggi, T. Pütterich, ITPA Integrated Operating Scenarios topical group, ASDEX Upgrade team, and JET Contributors, Nucl. Fusion **55**, 063031 (2015).

[3] A. Müller, Atoms **3**, 120 (2015).

[4] J. Rausch, A. Becker, K. Spruck, J. Hellhund, A. Borovik, Jr., K. Huber, S. Schippers, and A. Müller, J. Phys. B **44**, 165202 (2011).

[5] K. Spruck, N. R. Badnell, C. Krantz, O. Novotný, A. Becker, D. Bernhardt, M. Grieser, M. Hahn, R. Repnow, D. W. Savin, A. Wolf, A. Müller, and S. Schippers, Phys. Rev. A **90**, 032715 (2014).

[6] S. Schippers, D. Bernhardt, A. Müller, C. Krantz, M. Grieser, R. Repnow, A. Wolf, M. Lestinsky, M. Hahn, O. Novotný, and D. W. Savin, Phys. Rev. A **83**, 012711 (2011).

[7] A. Müller, S. Schippers, J. Hellhund, K. Holste, A. L. D. Kilcoyne, R. A. Phaneuf, C. P. Ballance, and B. M. McLaughlin, J. Phys. B **48**, 235203 (2015).

[8] M. S. Pindzola and D. C. Griffin, Phys. Rev. A **46**, 2486 (1992).

[9] R. G. Montague and M. F. A. Harrison, J. Phys. B **17**, 2707 (1984).

[10] M. Stenke, K. Aichele, D. Harthiramani, G. Hofmann, M. Steidl, R. Völpel, and E. Salzborn, J. Phys. B **28**, 2711 (1995).

[11] M. Stenke, K. Aichele, D. Harthiramani, G. Hofmann, M. Steidl, R. Völpel, V. P. Shevelko, H. Tawara, and E. Salzborn, J. Phys. B **28**, 4853 (1995).

[12] D.-H. Kwon, Y.-J. Rhee, and Y.-K. Kim, Int. J. Mass Spectrom. **252**, 213 (2006).

[13] C. P. Ballance, S. D. Loch, M. S. Pindzola, and D. C. Griffin, J. Phys. B **46**, 055202 (2013).

[14] M. S. Pindzola and D. C. Griffin, Phys. Rev. A **56**, 1654 (1997).

[15] D.-H. Zhangand D.-H. Kwon, J. Phys. B **47**, 075202 (2014).

[16] V. Jonauskas, A. Kynienė, G. Merkelis, G. Gaigalas, R. Kisielius, S. Kučas, Š. Masys, L. Radžiūtė, and P. Rynkun, Phys. Rev. A **91**, 012715 (2015).

[17] S. D. Loch, J. A. Ludlow, M. S. Pindzola, A. D. Whiteford, and D. C. Griffin, Phys. Rev. A **72**, 052716 (2005).

[18] A. V. Demura, M. B. Kadomtsev, V. S. Lisitsa, and V. A. Shurygin, JETP Lett. **101**, 85 (2015).

[19] V. Jonauskas, S. Kučas, and R. Karazija, Lith. J. Phys. **49**, 415 (2009).

[20] A. E. Kramida and T. Shirai, J. Phys. Chem. Ref. Data **35**, 423 (2006).

[21] A. E. Kramida and T. Shirai, At. Data Nucl. Data Tables **95**, 305 (2009).

[22] A. E. Kramida and T. Shirai, At. Data Nucl. Data Tables **95**, 1051 (2009).

[23] A. E. Kramida, Y. Ralchenko, J. Reader, and NIST ASD Team, Nist atomic spectra database (version 5.2), 2014.

[24] J. Jacobi, H. Knopp, S. Schippers, A. Müller, S. D. Loch, M. Witthoeft, M. S. Pindzola, and C. P. Ballance, Phys. Rev. A **70**, 042717 (2004).

[25] C. Becker, H. Knopp, J. Jacobi, H. Teng, S. Schippers, and A. Müller, J. Phys. B **37**, 1503 (2004).

[26] A. Borovik, Jr., A. Müller, S. Schippers, I. Bray, and D. V. Fursa, J. Phys. B **42**, 025203 (2009).

[27] P. Defrance, F. Brouillard, W. Claeys, and G. V. Wassenhove, J. Phys. B **14**, 103 (1981).

[28] A. Müller, K. Tinschert, C. Achenbach, R. Becker, and E. Salzborn, Nucl. Instrum. Methods B **10**, 204 (1985).

[29] A. Müller, K. Huber, K. Tinschert, R. Becker, and E. Salzborn, J. Phys. B **18**, 2993 (1985).

[30] A. Müller, K. Tinschert, G. Hofmann, E. Salzborn, and G. H. Dunn, Phys. Rev. Lett. **61**, 70 (1988).

[31] A. Müller, G. Hofmann, K. Tinschert, and E. Salzborn, Phys. Rev. Lett. **61**, 1352 (1988).

[32] A. Müller, G. Hofmann, B. Weissbecker, M. Stenke, K. Tinschert, M. Wagner, and E. Salzborn, Phys. Rev. Lett. **63**, 758 (1989).

[33] A. Borovik, Jr, M. F. Gharaibeh, P. M. Hillenbrand, S. Schippers, and A. Müller, J. Phys. B **46**, 175201 (2013).

[34] A. Müller, A. Borovik, Jr., K. Huber, S. Schippers, D. V. Fursa, and I. Bray, Phys. Rev. A **90**, 010701 (2014).

[35] R. Becker, A. Müller, C. Achenbach, K. Tinschert, and E. Salzborn, Nucl. Instrum. Methods Phys. Res., Sect. B **9**, 385 (1985).

[36] A. Borovik, Jr., M. F. Gharaibeh, S. Schippers, and A. Müller, J. Phys. B **48**, 035203 (2015).

[37] C. J. Fontes, H. L. Zhang, J. Abdallah, Jr., R. E. H. Clark, D. P. Kilcrease, J. Colgan, R. T. Cunningham, P. Hakel, N. H. Magee, and M. E. Sherrill, J. Phys. B **48**, 144014 (2015).

[38] Atomic and Optical Theory Group Los Alamos National Laboratory (LANL), Atomic physics codes package.
[39] A. Müller, Adv. At. Mol. Phys. **55**, 293 (2008).
[40] http://www-cfadc.phy.ornl.gov.
[41] R. D. Cowan, *The Theory of Atomic Structure and Spectra* (University of California Press, Berkeley, 1981).
[42] A. Müller, Int. J. Mass Spectrom. **192**, 9 (1999).
[43] M. Fogle, E. M. Bahati, M. E. Bannister, C. R. Vane, S. D. Loch, M. S. Pindzola, C. P. Ballance, R. D. Thomas, V. Zhaunerchyk, P. Bryans, W. Mitthumsiri, and D. W. Savin, Astrophys. J. Suppl. Ser. **175**, 543 (2008).
[44] C. H. Skinner, Phys. Scr. **T134**, 014022 (2009).
[45] T. Pütterich, Ph.D. thesis at Universität Augsburg, No 10/25, IPP Garching, Germany, 2006 .
[46] K. P. Dere, Astron. Astrophys. **466**, 771 (2007).